

In vitro ^1H MT and CEST MRI mapping of gastro-intestinal milk protein breakdown

Morwarid Mayar^{a,b}, Paul Smeets^{b,c}, John van Duynhoven^{a,*}, Camilla Terenzi^a

^a Laboratory of Biophysics, Wageningen University, Wageningen, the Netherlands

^b Division of Human Nutrition and Health, Wageningen University, Wageningen, the Netherlands

^c Image Sciences Institute, University Medical Center Utrecht, Utrecht University, Utrecht, the Netherlands

ARTICLE INFO

Keywords:

Magnetic Resonance Imaging
In vitro digestion
Protein coagulation
Chemical Exchange Saturation Transfer
Magnetization Transfer

ABSTRACT

Protein digestion is commonly studied using *in vitro* models. Validating these models with more complex *in vivo* observations remains challenging, in particular due to the need for non-invasive techniques. Here, we explore Magnetization Transfer (MT) and Chemical Exchange Saturation Transfer (CEST) MRI for non-invasive monitoring of protein solubilization and hydrolysis during static *in vitro* digestion using skim milk (SM). We measured CEST spectra of unheated and heated SM during gastric digestion, from which the relative amount of soluble proteins/peptides was estimated by calculating the asymmetric MT ratio (MTR_{asym}). We also obtained semi-solid volume fractions (v_{ss}), MT ratio (MTR) and MTR_{asym} from the same measurement, within 1.3 min. The MTR_{asym} area increased with gastric digestion, due to solubilization of the initially-formed coagulum, yielding a mean difference of $20 \pm 7\%$ between unheated and heated SM ($p < 0.005$). The v_{ss} and MTR decreased during gastric digestion and can be used to monitor changes in the coagulum, but not for assessment of soluble proteins/peptides. The MTR_{asym} increased for heated SM during gastro-intestinal digestion, proving sensitive to protein solubilization and hydrolysis, and is suitable for monitoring protein hydrolysis at later digestion stages. Future steps will include similar MT and CEST studies under dynamic conditions.

1. Introduction

Protein intake is essential for the growth and repair of body cells, muscle function and development of the immune system. Milk is one of the main sources of protein in the human diet and is the only source of protein for infants. Milk proteins, namely casein and whey, are digested in the gastro-intestinal tract, which is a complex dynamic system and is crucial for the breakdown of milk proteins and for the subsequent absorption of amino acids (Dupont & Tomé, 2014). Milk protein digestion starts in the gastric phase (GP), where first a semi-solid protein coagulum is formed by a combination of acid- and pepsin-induced aggregation of the casein micelles or, in the case of heated milk, of casein micelles and denatured whey proteins (Huppertz & Chia, 2021). This is followed by solubilization and hydrolysis of the semi-solid protein coagulum into soluble proteins and relatively large peptides. Next, these proteins and peptides are transported into the intestinal phase (IP), where they are hydrolyzed into small peptides and amino-acids (Dupont & Tomé, 2019). Processing of milk products frequently includes heating, which in turn can modify the structure, gastric coagulation, and overall

digestibility of the proteins (Huppertz & Chia, 2021; van Lieshout et al., 2020). Protein digestion is currently studied using either animal models (Barbé et al., 2014), static (Brodkorb et al., 2019; Ménard et al., 2018) or (semi)-dynamic *in vitro* digestion models (Dong et al., 2021; Mulet-Cabero, Egger, et al., 2020; Mulet-Cabero et al., 2017), gastric aspirates in infants (Nielsen et al., 2020), ileal sampling (Gaudichon et al., 1999) or by measuring the appearance of amino acids in blood in humans (Bos et al., 2003; Horstman et al., 2021). *In vitro* digestion models are useful because they are simple, well controlled, do not impose any ethical constraints, and can provide insights into the digestion kinetics and chemical composition of the digesta. However, they need to be validated using *in vivo* data. This requires the use of non-invasive measurement techniques that can monitor both *in vitro* and *in vivo* digestion.

Magnetic Resonance Imaging (MRI) has great potential for investigating *in vivo* protein digestion because it can be used to acquire detailed images of the gastro-intestinal tract in a non-invasive manner (Smeets et al., 2020). MRI is currently mainly used to assess gastric processes, such as gastric emptying and phase separation, at a macroscopic level

* Corresponding author.

E-mail address: john.vanduynhoven@wur.nl (J. van Duynhoven).

<https://doi.org/10.1016/j.foostr.2023.100314>

Received 26 September 2022; Received in revised form 18 January 2023; Accepted 9 February 2023

Available online 14 February 2023

2213-3291/© 2023 The Author(s). Published by Elsevier Ltd. This is an open access article under the CC BY license (<http://creativecommons.org/licenses/by/4.0/>).

(Camps, Mars, de Graaf, & Smeets, 2017; Spiller & Marciani, 2019; Camps et al., 2021). While macroscopic MRI images can provide some information on the degree of coagulation, as apparent visually, they do not provide a local molecular-scale measure of the degree of milk protein coagulation and protein breakdown.

Previous studies have shown that the ^1H longitudinal (R_1) and transverse (R_2) Nuclear Magnetic Resonance (NMR) relaxation rates can be used to monitor the digestion of whey protein gels in a static (Deng et al., 2020) and semi-dynamic (Deng et al., 2022) *in vitro* gastric digestion model. The R_1 and R_2 parameters provide information on the molecular mobility of water in food systems, but their translation into quantitative chemically-specific or molecular-level parameters is not trivial. Magnetization Transfer (MT) and Chemical Exchange Saturation Transfer (CEST) are promising MRI techniques for monitoring milk protein coagulation and breakdown on a macroscopic- and (supra-) molecular level. MT is a magnetic resonance technique that can be used to quantify low-abundant semi-solid proteins in aqueous foods *via* through-space dipolar couplings and ^1H exchange between the semi-solid protein and water (Henkelman et al., 1993; van Duynhoven et al., 1999). CEST is based on the same principle as MT, but instead it can be used to measure the ^1H chemical exchange between amide, amine and hydroxyl protons of dissolved and mobile proteins/peptides and water (Van Zijl & Yadav, 2011). CEST is known to be dependent on solute concentration (Chan et al., 2014), molecular conformation (e.g. protein folding/unfolding and structural rearrangements) (Goerke et al., 2015; Longo et al., 2014a) and pH (Sun et al., 2016). Therefore, a combination of MT and CEST MRI is promising for the assessment of both semi-solid and soluble proteins during gastric digestion. MT and CEST measurements are performed using the same MRI pulse sequence. First a radio-frequency (RF) saturation pulse is applied at a frequency offset relative to the water signal. This pulse selectively saturates the magnetization of protons associated with the semi-solid macromolecules or solutes by equalizing the populations of the respective ^1H energy levels. The obtained saturation is then transferred to the water protons *via* a combination of through-space dipolar couplings and ^1H chemical exchange. The saturation transfer can then be detected as a suppression of the water signal. The saturation pulse can be applied at both positive and negative frequency offsets (Δ) relative to the water proton frequency to acquire a CEST spectrum. In the CEST spectrum the water signal intensity with the saturation pulse applied at a given Δ value ($S_{\text{sat}}(\Delta)$) is normalized to the signal intensity without any saturation (S_0), and is plotted as a function of the frequency offset Δ . The CEST spectrum includes contributions from ^1H chemical exchange with mobile low-molecular-weight molecules, MT with semi-solid molecules and direct water saturation (DS) (Van Zijl & Yadav, 2011; Wu et al., 2016). From the CEST spectrum, the MT ratio (MTR) (Eq. 1) and the MTR_{asym} (Eq. 2) can be obtained, as follows:

$$MTR = 1 - (S_{\text{sat}}(\Delta)/S_0) \quad (1)$$

$$MTR_{\text{asym}} = (S_{\text{sat}}(-\Delta) - S_{\text{sat}}(+\Delta))/S_0 \quad (2)$$

The MTR parameter is mainly dependent on the amount of semi-solid protein and the ^1H exchange rate. We have previously shown that bulk NMR measurements of the MTR can be used to monitor the *in vitro* gastric coagulation and breakdown of milk proteins and to study the effect of heating on this process (Mayar et al., 2022). The chemical exchange of soluble proteins/peptides can be identified by the MTR_{asym} calculation, which removes the additional semi-solid MT and DS contributions from the CEST spectrum. This calculation is based on the assumption that the MT and DS contributions are symmetric around the water signal, but the chemical exchange effect is asymmetric (Van Zijl & Yadav, 2011). *In vitro* gastro-intestinal protein digestion includes changes in the state of proteins, such as coagulation, solubilization and hydrolysis (Huppertz & Chia, 2021; Mulet-Cabero, Egger, et al., 2020). Therefore, we hypothesize that a combination of CEST and MT MRI can

be used to monitor these changes during static *in vitro* infant gastro-intestinal digestion of milk. In the present study, we combine CEST and MT measurements with imaging to obtain spatially-resolved information on *in vitro* milk protein coagulation and breakdown. The infant *in vitro* digestion protocol was chosen because milk is the only source of protein for infants but the effect of heating on gastric protein digestion is still poorly understood in this group. Gaining a better understanding of the effect of processing on digestion can aid in optimizing the production process of infant formula for optimal protein digestion. The methodology described in this paper can however directly be applied to other digestion models, such as INFOGEST (Brodtkorb et al., 2019).

2. Materials and methods

2.1. Materials

Whey Protein Isolate (WPI) was purchased from Davisco Food International, Inc. (USA). Pepsin (631 U/mg), pancreatin (trypsin activity 3.13 U/mg) from porcine origin, trypsin (10,000 U/mg) and bile from bovine origin, trypsin inhibitor (Pefabloc), calcium chloride hexahydrate, hydrochloric acid, L-serine, potassium chloride, sodium bicarbonate, sodium chloride, sodium hydroxide and tris(hydroxymethyl) aminomethane hydrochloride were all purchased from Sigma Aldrich, Inc. (USA). Pepsin inhibitor (pepstatin A) was purchased from Thermo Scientific, Inc. (USA). O-phthaldehyde (OPA), disodium tetraborate decahydrate, sodium dodecyl sulfate (SDS), dithiothreitol (DTT) were purchased from Merck (Germany). Milli-Q water (resistivity 18.2 M Ω .cm at 25 °C, Merck Millipore, USA) was used in all experiments.

2.2. Preparation of WPI solutions

WPI powder was dissolved in Milli-Q water at different concentrations (1, 3, 6, 12 wt%) and stirred at room temperature (RT) for 1 h. The pH of the solutions was adjusted to pH 2, 3.5, 4.5, 5, 5.5 and 7 using either 1 M hydrochloric acid or 0.1 M sodium hydroxide. The protein solutions were stored in the fridge at 5 °C and were used within one day. The WPI solutions were prepared and measured in duplicate.

2.3. Preparation of whey protein hydrolysate

Whey protein concentrate (WPC) powder was obtained from raw skim milk (SM) from bovine origin. The SM was acidified with 1 M hydrochloric acid to a pH of 4.6 to precipitate the casein micelles, followed by centrifugation for 20 min at 4 °C and 6000 g. The supernatant containing the soluble whey proteins was separated from the pellet and was dialyzed to remove salts and lactose. The dialysis was performed against a solution of lactic acid in Milli-Q at pH 4.6 and 4 °C using a dialysis membrane with a molecular weight cutoff of 10 kDa. The demineralized whey protein was freeze dried to obtain the WPC powder. The WPC powder was dissolved in TRIS-HCl (3.4 wt%) and the pH was adjusted to pH 7.5 using 0.1 M sodium hydroxide. The WPC solution was incubated with 5 mg of trypsin per gram of protein at 45 °C for 2.5 and 5.5 h to obtain the whey protein hydrolysate. The WPC hydrolysate samples were prepared and measured in duplicate.

2.4. Preparation of simulated digestion fluids

Simulated gastric fluid (SGF) was composed of sodium chloride and potassium chloride with a concentration of 94 and 13 mM, respectively, and adjusted to pH 5.3. Pepsin was added to SGF right before the digestion experiment. Simulated intestinal fluid (SIF) was composed of 164 mM sodium chloride, 10 mM potassium chloride and 85 mM of sodium bicarbonate and adjusted to pH 7. Calcium chloride was added separately before the beginning of the intestinal phase at a concentration of 3 mM within the volume of the intestinal fluid.

2.5. *In vitro* digestion

Raw and heated SM were obtained following a procedure described elsewhere (Mayar et al., 2022). *In vitro* gastric and intestinal digestion was conducted based on a digestion protocol for 1 month old infants (Ménard et al., 2018). To prepare 1 mL of gastric digestion sample, SM and SGF containing pepsin were mixed in a 10-mm NMR tube in a 63:37 (v/v) ratio. The activity of pepsin in the digestion sample was 268 U/mL of gastric content. The pH was adjusted to 5.3 with 1 M hydrochloric acid. The samples were incubated in a water bath at 37 °C for $t = 0, 1, 5, 15, 30$ and 60 min. These time points were based on (Ménard et al., 2018) with the addition of $t = 1$ min to better capture the fast disappearance of the coagulum in raw SM. The activity of pepsin was inhibited by adding 10 μ L of a 0.72 μ M Pepstatin A solution. The samples were measured by MRI without any further sample preparation. For intestinal digestion, first 5 mL of $t = 60$ min gastric digestion sample was prepared. The pH was adjusted to pH 6.6 and the sample was mixed with SIF in a 62:38 (v/v) ratio to obtain intestinal digestion samples composed of 39% SM, 23% SGF and 38% SIF. The SIF contained pancreatin with a trypsin activity of 16 U/mL of intestinal content. The samples were incubated in a water bath at 37 °C for $t = 0, 1, 5, 15, 30$ and 60 min. The activity of trypsin was stopped by adding 10 μ L of a 0.5 M Pefabloc solution. Both gastric and intestinal digestion experiments were performed in triplicate.

2.6. MRI measurements

^1H CEST MRI measurements were conducted at RT at a magnetic field strength of 7 T, corresponding to a ^1H frequency of 300.13 MHz, on an Avance III spectrometer (Bruker Biospin, Fallanden, Switzerland) equipped with the Micro 2.5 radiofrequency (RF) coil with an inner diameter of 30 mm and the Micro 2.5 microimaging gradient system with maximum gradient intensity of $1.5 \text{ T}\cdot\text{m}^{-1}$ along all three axes. Measurements were conducted using a CEST-Rapid Acquisition with Refocused Echoes (RARE) sequence. The CEST module consisted of a train of 10 block pulses with a pulse length (t_p) of 100 ms and an interpulse delay (t_{delay}) of 10 μ s, resulting in a saturation time (T_{sat}) of 1 s. The B_1 amplitude was set to 3 μ T. ^1H CEST spectra were measured for 61 Δ values equally spaced from -10 to 10 ppm, yielding a CEST spectral resolution of 0.33 ppm. Water saturation shift referencing (WASSR) (Kim et al., 2009) spectra were measured to construct a B_0 -map for B_0 -inhomogeneity correction of the CEST spectra. For the WASSR measurement, a T_{sat} of 50 ms and a B_1 of 0.2 μ T was used. The saturation pulse consisted of 10 block pulses with a t_p of 5 ms and a t_{delay} of 10 μ s. WASSR spectra were measured using 31 Δ values ranging between -1.5 and 1.5 ppm with a resolution of 0.1 ppm. In addition, two reference S_0 images were acquired, respectively at $\Delta = -450$ and 450 ppm. The RARE imaging parameters were as follows: field-of-view of 25×25 mm, matrix size of 128×128 , three axial slices with thickness of 2 mm, distance of 3 mm and offset set to -3 mm. Sinc3 pulses were used for excitation and refocusing with a flip angle of 90° and 180°, respectively. A repetition time (TR) of 5 s, echo time (TE) of 9.8 ms, RARE-factor of 32 and number of averages (NA) of 1 was used, resulting in a total acquisition time of 21 min and 11 min for the CEST and WASSR measurement, respectively. The effective TE was 78 ms, leading to a T_2 -weighted image in which the signal of semi-solid protons with a short transverse relaxation time (T_2) is suppressed.

2.7. Data processing and analysis

All processing and calculations were done in MATLAB R2019b (MathWorks, Massachusetts, USA). First, WASSR spectra were constructed for each voxel by calculating S_{sat}/S_0 as a function of Δ . The WASSR spectra were interpolated with cubic-spline fitting on a voxel-by-voxel basis and the frequency shift, $\delta\Delta^{\text{WASSR}} = \Delta_{\text{min}} - \Delta_0$, was

determined for each voxel as the difference between the position for the minimum of the interpolated spectrum, Δ_{min} , and the reference position of the water signal, $\Delta_0 = 0$ ppm. The WASSR B_0 -map was constructed by plotting $\delta\Delta^{\text{WASSR}}(x,y)$ for each voxel. Next, the CEST saturation frequencies were corrected voxel-wise by using the WASSR B_0 -map and the S_{sat} images were then interpolated with cubic-spline fitting to obtain the S_{sat} signal intensity at the desired Δ . Region-of-Interest (ROI) masks of the sample tube were drawn manually, and the mean signal intensity within the ROI was used to construct the CEST spectra, where S_{sat}/S_0 is plotted as a function of Δ . The MTR and MTR_{asym} were calculated according to Eqs. 1 and 2. The MTR_{asym} area was calculated as the area under the curve between 1.2 and 4 ppm. For WPI, WPC and milk digestion samples, the mean CEST and corresponding MTR_{asym} spectra were calculated per slice over the whole sample tube. The WPI and WPC samples were homogenous solutions, therefore, calculating the mean CEST and MTR_{asym} spectra over the sample tube is adequate and gives a good representation of the local MTR_{asym} . For the milk digestion samples, which are heterogenous, additional semi-solid and liquid content masks were obtained by intensity thresholding of the T_2 -weighted S_0 images using the multithresh function with two levels in Matlab. Masks for the semi-solid or the liquid phases in the sample were applied to the unsaturated and saturated images in order to calculate the MTR and MTR_{asym} maps of the coagulum and supernatant, respectively. The masks for the solid-phase sample components were also used to calculate the semi-solid volume (v_{ss}) by multiplying the voxel volume by the total number of solid-containing voxels. The mean MTR and MTR_{asym} values were calculated by taking the sum over either the solid- or liquid-containing voxels, and averaging it over the total number of voxels within the respective ROIs.

2.8. OPA assay

The degree of hydrolysis of WPC hydrolysate samples was determined using the OPA method (Nielsen et al., 2001). First the OPA reagent solution was prepared by dissolving 3.8 g disodium tetraborate decahydrate in 80 mL of MilliQ while stirring at 35–40 °C. Next, 88 mg DTT and 100 mg SDS were added. Then, 80 mg OPA was dissolved in 3 mL ethanol and transferred to the above-mentioned solution and the volume was adjusted to 100 mL with Milli-Q. The WPC samples were centrifuged at 10,000 g for 30 min and diluted 10 times. The calibration curve consisted of L-serine standards of 0.5, 1.25, 2.5, 5, 7.5, 10 and 15 mM in MilliQ. To prepare the samples for measurement, 10 μ L of the blank (Milli-Q), L-serine standard or diluted WPC sample was added to a well of a transparent 96-well polystyrene plate (Greiner) and was mixed with 200 μ L of OPA reagent. The well-plate was covered with aluminum foil and kept at RT for 15 min. The absorbance was measured at 340 nm using a Spectramax M2 microplate reader. The degree of hydrolysis (DH) was calculated using the method described by Spellman et al. (Spellman et al., 2003).

2.9. Statistical analysis

The means and standard deviations were calculated based on duplicate or triplicate experiments. The error bars in the figures represent the standard deviations. The regression analysis for the MTR_{asym} area with the pH and protein concentration were performed in MATLAB R2019b (MathWorks, Massachusetts, USA) using the “fit linear regression model” function. Repeated measures analysis of variance (repeated measures ANOVA) followed by a Post-hoc Tukey’s honestly significant difference (HSD) test was performed in MATLAB to determine whether there was a significant effect of digestion time and heat treatment on the MTR_{asym} area. The significance level for all analyses was set at $p = 0.05$.

3. Results and discussion

3.1. ^1H CEST of WPI and WPC solutions: effect of pH, concentration and hydrolysis

The effect of pH and protein concentration on the chemical exchange was studied using WPI solutions at varying pH (Fig. 1a-c) and concentration (Fig. 1d-f). The CEST spectra at different pH (Fig. 1a) contain a broad and symmetric direct saturation (DS) of the water signal at 0 ppm and a CEST signal around 3 ppm. The CEST signal is the result of chemical exchange between water protons and the exchangeable protein protons, such as hydroxyl ($\sim\Delta = 1$ ppm), amine ($\Delta = 2-3$ ppm) and amide ($\Delta = 3.5$ ppm) protons (DeBrosse et al., 2016; Pardi et al., 1983).

The MTR_{asym} spectra were calculated for better quantification of chemical exchange (Fig. 1b): their amplitude increases with pH, most significantly between pH 2 and 3.5 and pH 5.5 and 7. The MTR_{asym} spectra at pH 3.5–5.5 have a similar shape and intensity with two overlapping peaks at ~ 1 and 2.5 ppm, and are notably different as compared to the spectrum at pH 7. We note that the samples at pH 3.5–5.5 were more turbid as compared to those prepared at pH 2 and 7 (Fig. S1), indicating a correspondingly lower solubility and/or aggregation of the whey proteins. The pH range 3.5–5.5 is near the iso-electric point (pI) of bovine whey proteins, namely around pH 4.2 or 5.1 for α -lactalbumin or β -lactoglobulin, respectively. Proteins are known to aggregate, and are less soluble at their pI (Cornacchia et al., 2014), which might explain the distinct shape and low intensity of the MTR_{asym} spectrum in this pH range. These observations are in agreement with CEST data of bovine serum albumin, where a decrease in the MTR_{asym} and a separation into two peaks was observed upon heat-induced aggregation (Longo et al., 2014b).

The area under the MTR_{asym} spectrum between $\Delta = 1.2-4$ ppm was calculated to quantify the pH dependence of the bulk chemical ex-

change. We note that $\Delta < 1$ ppm ranges were excluded in this calculation because, at Δ values close to the direct water saturation condition around 0 ppm, the MTR_{asym} analysis becomes unreliable and the MTR_{asym} intensity depends on the slice position, even for homogenous whey protein solutions (Fig. S2). We find that the area under the MTR_{asym} spectrum follows a linearly increasing trend with pH (Fig. 1c), with smaller differences and overlapping error bars observed in the pH range around the pI of the whey proteins. Chemical exchange is a dominantly base-catalyzed reaction, which explains the increase of the MTR_{asym} with pH.

The CEST signal and MTR_{asym} also increased with concentration (Fig. 1d-f), while the shape of the MTR_{asym} remained the same for all concentrations. These results show that the MTR_{asym} is sensitive to variations in pH and protein concentration, which can occur during *in vivo* protein digestion (Gan et al., 2018). However, the main changes expected to occur during static *in vitro* digestion are protein solubilization and hydrolysis.

To verify whether CEST is sensitive to protein hydrolysis, a whey protein hydrolysate was prepared by incubating an unheated intact WPC solution with trypsin at pH 7.5 at 45 °C for 2.5 and 5.5 h. Unheated WPC was used to avoid whey protein denaturation and aggregation, which could both cause variations in the chemical exchange.

As shown in Fig. 2a, the CEST spectra for the intact or hydrolyzed samples are very similar, with only a small difference observed in the $\Delta = 0.6-3.5$ ppm range. This difference is more clearly visualized in Fig. 2b in the MTR_{asym} spectral representation, where a gradual increase is observed with the hydrolysis time. During protein hydrolysis, the peptide bonds are broken and more free hydroxyl (~ 1 ppm) and amine ($2-3$ ppm) groups are formed, thus yielding an increased abundance of exchangeable protons. This explains the strong increase in the MTR_{asym} occurring between 1 and 3 ppm. The increase in the MTR_{asym} area is 22

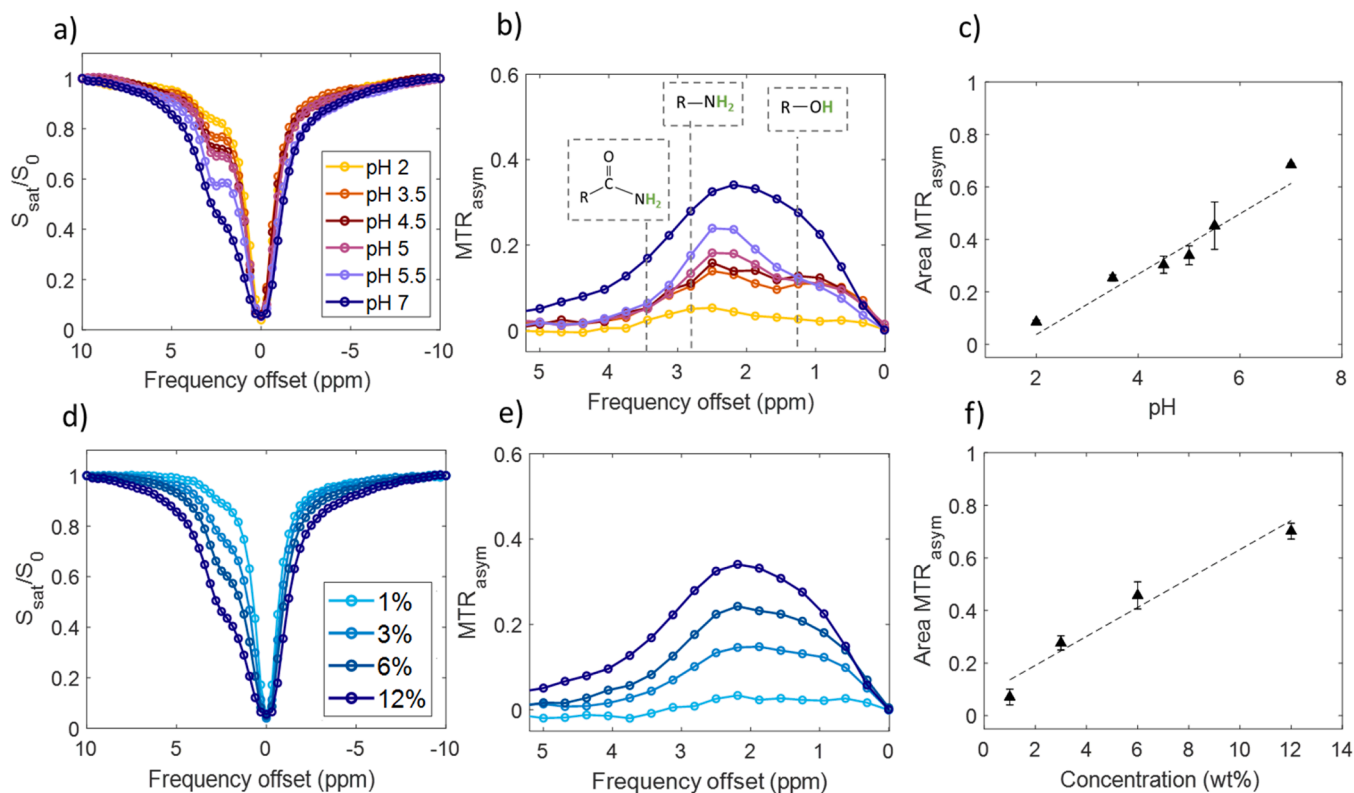


Fig. 1. For WPI solutions at 12% concentration and varying pH (a-c) or at pH 7 and varying concentration (d-f): ^1H CEST (a, d) and MTR_{asym} spectra (b, e), alongside the respective correlation plots for the normalized MTR_{asym} areas ($\Delta = 1.2-4$ ppm) as a function of either pH ($y = 0.11x - 0.16, R^2 = 0.94$) (c) or concentration ($y = 0.07x + 0.05, R^2 = 0.94$) (f). The MTR_{asym} area values are plotted as the mean \pm SD of duplicate experiments.

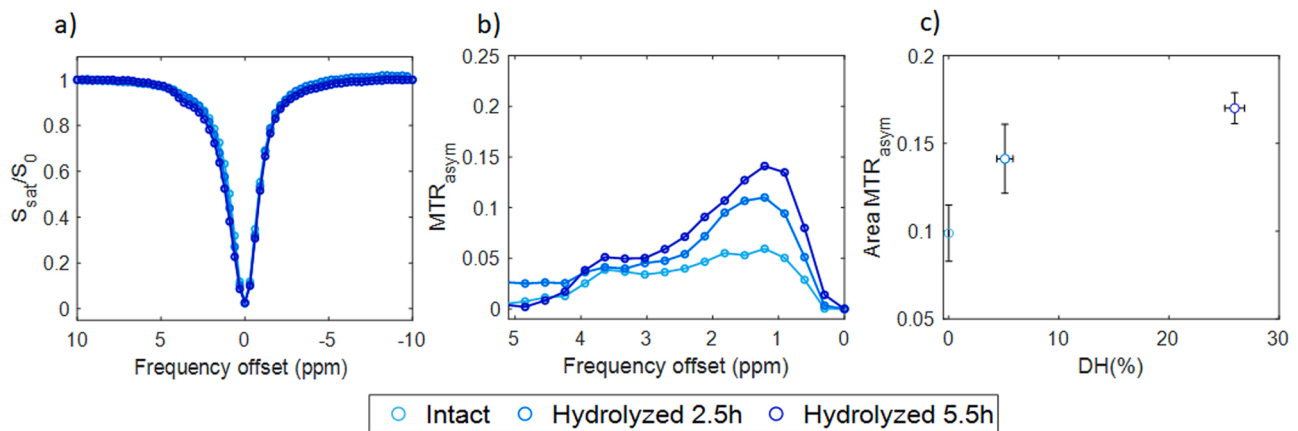


Fig. 2. CEST (a) and MTR_{asym} (b) spectra and the DH (%) determined with the OPA assay (c) for intact 3.4% WPC solution and after 2.5 and 5.5h of hydrolysis. The hydrolysis was performed with trypsin (0.5%) at pH 7.5 and 45 °C.

$\pm 1\%$ and $35 \pm 1\%$ for 2.5 and 5.5 h of hydrolysis, respectively, which is in agreement with the trend observed for the degree of hydrolysis (Fig. 2c). The degree of hydrolysis after 5.5 h is quite extensive ($26 \pm 1\%$), which is expected considering the extreme conditions used. The

results shown in Figs. 1 and 2 demonstrate that CEST is sensitive not only to pH and protein concentration, but also to protein hydrolysis.

3.2. ^1H CEST MRI of gastric milk protein digestion

Next, CEST was used to monitor the *in vitro* digestion of unheated SM

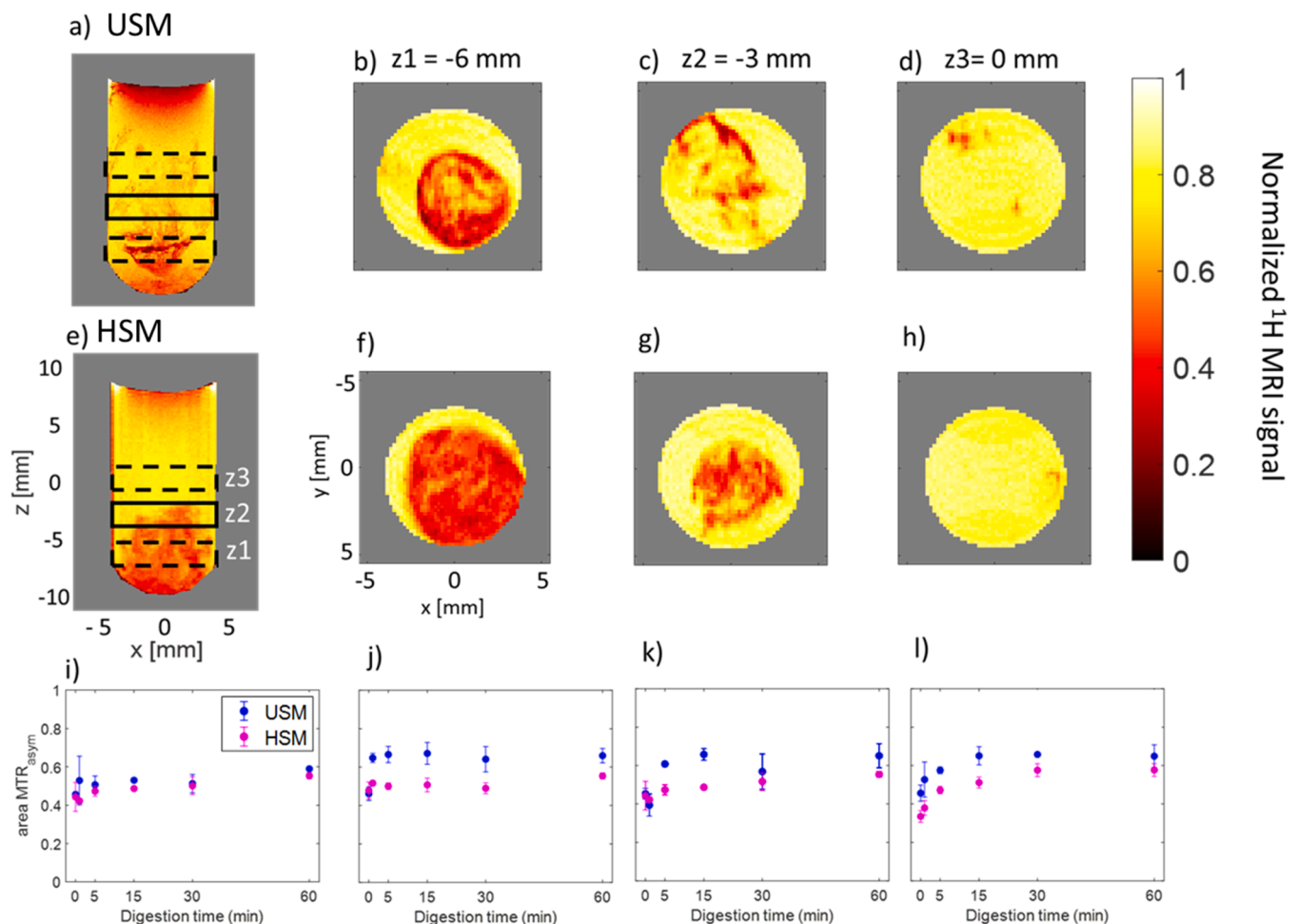


Fig. 3. T_2 -weighted ^1H MRI intensity images at $t = 15$ min of USM (a-d) and HSM (e-h) acquired for a sagittal slice (a and e) or for three axial slices (b-d and f-h) at z -coordinate set to -6 mm (b and f), -3 mm (c and g) or 0 mm (d and h), alongside the digestion time evolution for the MTR_{asym} area for the bulk sample (i) or for three axial slices (j-l). The slice thickness was 2 mm for the sagittal and axial measurements. The coagulum is visible in red and the supernatant in yellow. The MTR_{asym} area was calculated from the CEST spectrum between 1.2 and 4 ppm, and is plotted as the mean \pm SD of triplicate digestion experiments.

(USM) and heated SM (HSM), which contain both whey proteins and caseins. During gastric digestion, phase separation between the milk protein coagulum and its supernatant was observed. This can be detected also in Fig. 3, where the sagittal and axial ^1H T_2 -weighted S_0 -images of the CEST measurement for both USM (a-d) and HSM (e-h) are shown. Water molecules in the protein coagulum are less mobile and, hence, have a shorter T_2 relaxation time compared to those in the supernatant. As a consequence, the protein coagulum and its supernatant have a respectively lower (red) or higher (yellow) ^1H signal intensity in the T_2 -weighted images. We note that semi-solid proteins cannot be detected directly in the T_2 -weighted images, because of their very short T_2 relaxation time in the order of 12–20 μs (Mayar et al., 2022). The CEST and MTR_{asym} spectra were averaged over the whole slice to obtain information on the global changes occurring during *in vitro* digestion for the whole sample composition (coagulum and supernatant).

There was no clear trend as a function of the digestion time for the CEST spectra of the digestion samples, shown in supplementary Figs. S3 and S4. The MTR_{asym} spectra for the bottom slice, whose ^1H signal mainly arises from the protein coagulum, remain unchanged during digestion, with a slight intensity increase occurring only between $t = 0$ and 1 min. Unlike for the coagulum, the middle and top slice exhibit an observable increase in the MTR_{asym} spectral intensity during digestion, with a difference in peak intensity of 0.2 between $t = 0$ and $t = 60$ min. As shown in Fig. 3i-l, these variations are better visualized by monitoring the evolution of the MTR_{asym} area with digestion. The MTR_{asym} area for the bulk sample and the bottom slice (Fig. 3i,j) remains unchanged as digestion progresses, with only a slight variation observed between $t = 0$ and 1 min in the bottom slice for unheated SM. A clearer variation with digestion is observed for the middle and top slice (Fig. 3k, l).

The largest variation with digestion and heat treatment is observed for the top slice, which mainly consists of the supernatant. During digestion, the MTR_{asym} spectra of the supernatant (Fig. S3 and S4) increased between 1 and 4 ppm, corresponding to the resonance positions of hydroxyl, amine and amide protons. Bovine milk mainly consists of caseins, which lack a well-defined secondary structure and are mainly present as random coils in aqueous solutions (Bhat et al., 2016). Moreover, the pH of the samples over the different digestion time points ($\text{pH} = 5.43 \pm 0.04$) and the measurement temperature (RT) were constant. Therefore, conformational changes in the secondary structure are unlikely (Bhat et al., 2016; Markoska et al., 2021; Pardi et al., 1983) and can be ruled out as a cause of variations in the chemical exchange. The observed increase in the MTR_{asym} can therefore be attributed to solubilization of the protein coagulum, which leads to more proteins and, hence, to more exchangeable protons in the liquid phase. The larger increase observed specifically at 1.2 ppm (hydroxyl) and 2–3 ppm (amine) could be due to hydrolysis of the peptide bonds, which leads to more free amine and hydroxyl groups. The increase in the MTR_{asym} area between $t = 1$ and 60 min was 20% and 35% for unheated and heated SM, respectively. During gastric digestion, pepsin hydrolyzes the peptide-bonds in the semi-solid protein coagulum, which results in proteins and peptides being released from the coagulum into the supernatant. This is expected to lead to a higher concentration of proteins and peptides and, hence, of exchangeable protons in the supernatant, which explains the observed increase in the MTR_{asym} area within the top imaging slice. Dominant effects of digestion time ($F(5,2) = 80$, $p < 0.001$) and heat treatment ($F(1,2) = 200$, $p < 0.005$) were observed on the MTR_{asym} of the top slice as found by a repeated measures ANOVA. A *post hoc* comparison with Tukey's HSD test showed that the mean value of the MTR_{asym} was significantly different between USM and HSM for all digestion time points ($p < 0.05$). For the bottom and middle slice, this variation is smaller because, while the amount of semi-solid proteins decreases, and therefore the amount of soluble proteins and peptides increases, there are no large changes in the net protein concentration.

Overall these results show that the MTR_{asym} area is a MRI parameter sensitive to static *in vitro* digestion and, hence, is potentially useful for monitoring *in vivo* protein digestion. However, the acquisition of a full CEST spectrum is time consuming, here taking up to about 21 min for sampling a total of 61 frequency offset values, including 2 reference images (see Section 2.5). Such long measurement times prohibit the implementation of CEST measurements on a clinical scanner for dynamic studies of *in vivo* protein digestion. To address this limitation, we investigated whether the MTR_{asym} obtained from one set of $\pm\Delta$ values could be used to construct MTR_{asym} contrast maps as a function of digestion time, which would require 1 min and 20 s of acquisition time and thus enable a ~ 16 -fold faster measurement. Moreover, the measurement of each Δ is 20 s, and hence, fits within one breath hold, which is important for avoiding breathing-related artifacts in the images.

In Fig. 3, we observed that changes in the MTR_{asym} during protein digestion were best detected in the top imaging slice, mainly consisting of supernatant. Therefore, MTR_{asym} maps of the supernatant in the middle slice ($z = -3$ mm) were constructed for the exchangeable hydroxyl ($\Delta = 1.2$ ppm) or amine ($\Delta = 2$ and 2.7 ppm) protons (Fig. 4a). The T_2 -weighted images shown in Fig. 3 were used as a reference to obtain an image mask for the supernatant and coagulum ^1H MRI signals by intensity thresholding. The values in the MTR_{asym} maps of the supernatant were normalized to the highest value in the respective map. The contrast maps show that the MTR_{asym} for the supernatant at $\Delta = \pm 2.7$ ppm exhibits the largest variation upon digestion, as indicated by the clear shift from low (red) to high (yellow) MTR_{asym} values. Fig. 4b shows the mean MTR_{asym} for the supernatant calculated using the respective image mask. At $\Delta = \pm 2.7$ ppm the mean MTR_{asym} exhibits only a slightly better variation with digestion as compared to ± 1.2 and ± 2.0 ppm. Nevertheless, $\Delta = \pm 2.7$ is a more optimal offset for monitoring digestion due to the larger difference with respect to the water saturation signal at 0 ppm, which is especially important for application on clinical scanners with a lower magnetic field of 3 T. Therefore, offset values of ± 2.7 ppm were chosen for monitoring *in vitro* protein digestion of USM and HSM in the gastric phase (GP) and of HSM in the intestinal phase (IP).

3.3. T_2 -weighted, MTR and MTR_{asym} imaging of protein digestion

In the following, the use of MTR_{asym} , T_2 -weighted and MTR-contrast ($\Delta = 2.7$ ppm) images is tested for monitoring protein digestion in the gastric phase for USM (GP-USM) and HSM (GP-HSM), as well as in the intestinal phase for HSM (IP-HSM) (Fig. 5a-c). The water phase inside the coagulum and supernatant can clearly be distinguished in the T_2 -weighted images of Fig. 5a, and it is possible to visually trace the breakdown of the protein coagulum as digestion progresses for GP-USM and GP-HSM systems. We note that, as expected, the coagulum in IP-HSM is absent even at the start of intestinal digestion. These images can be used to estimate changes in the apparent semi-solid volume, v_{ss} , within the samples, which in turn can be used as a measure of the changes in the amount of protein coagulum. Here, we refer to the coagulum as a semi-solid, because this is a term commonly used in MT and CEST MRI literature to refer to hydrated (bio)-polymers, akin to the casein coagulum (Mayar et al., 2022; van Zijl et al., 2018). It is important to note that exact measurements of the semi-solid volume are not possible, due to partial volume effects in the slice direction and the image acquisition parameters used, namely slice thickness and gap of 2 and 1 mm, respectively. As shown in Fig. 5d, for both USM and HSM, v_{ss} decreased during gastric digestion, due to the breakdown of the protein coagulum.

The MTR maps in Fig. 5b are clearly affected by variations in the amount of semi-solid protons, and can be used to selectively characterize the protein coagulum and to trace its breakdown. The mean MTR (Fig. 5e) decreases with digestion in a similar fashion as the solid

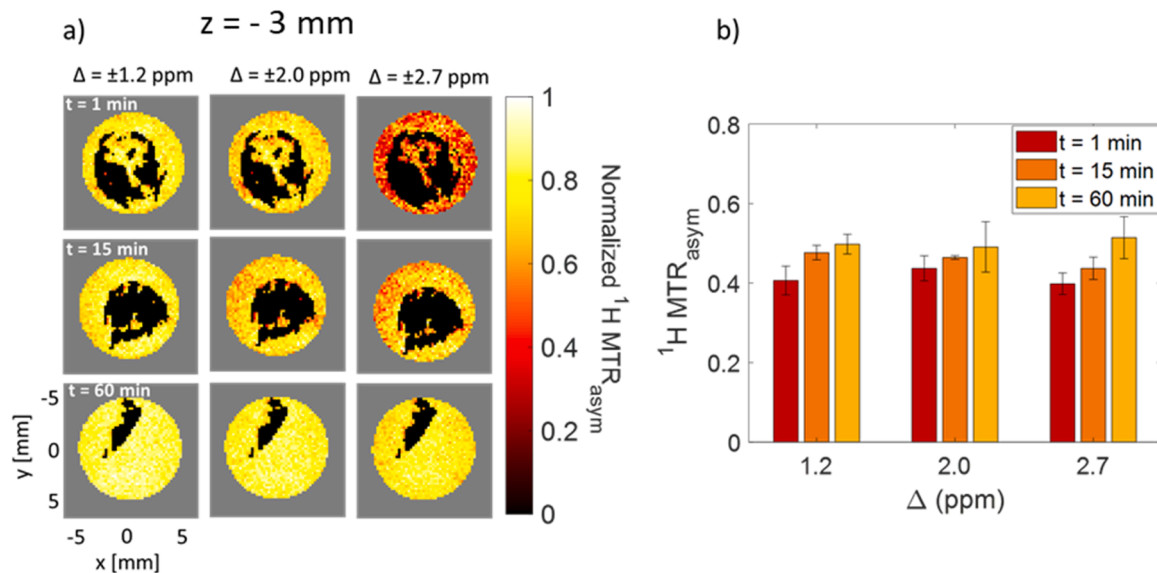


Fig. 4. Normalized axial ($z = -3$ mm) MTR_{asym} contrast maps at $\Delta = 1.2$ (left), 2.0 (middle), or 2.7 ppm (right) and at $t = 1$ (top), 15 (middle) and 60 min (bottom) gastric digestion times (a); mean $MTR_{asym} \pm$ SD ($n = 3$) for each Δ and timepoint calculated over the voxels containing the supernatant (b). The values in (b) are the mean MTR_{asym} values whereas the maps in (a) show the MTR_{asym} values, normalized to the maximum value within each map, for the voxels containing the supernatant as obtained by thresholding of the T_2 -weighted images shown in Fig. 3.

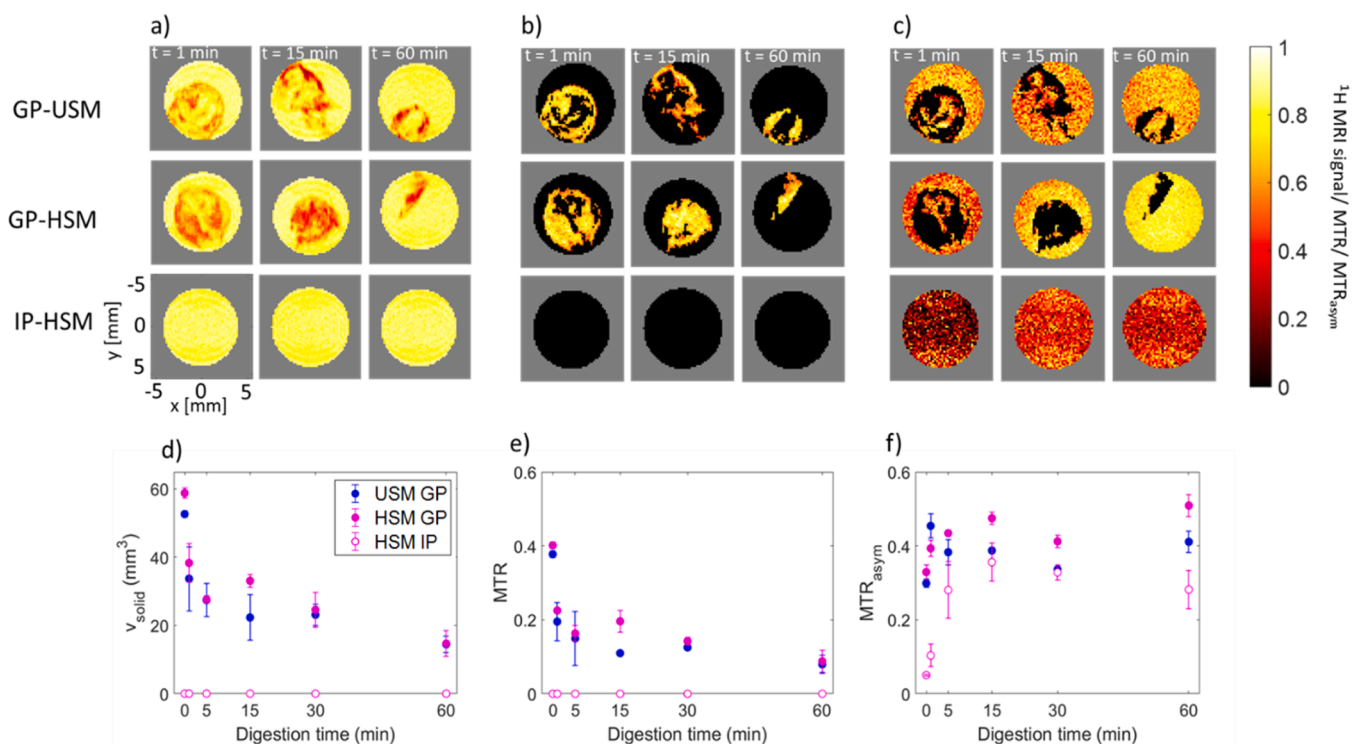


Fig. 5. For GP-USM (top a-c or filled blue circles d-f), GP-HSM (middle a-c or filled pink circles d-f) and IP-HSM (bottom a-c or empty pink circles d-f): normalized axial ($z = -3$ mm) T_2 -weighted ^1H intensity images (a), alongside MTR (b) and MTR_{asym} maps both at $\Delta = 2.7$ ppm (c); digestion time evolution for v_{ss} (d), mean MTR (e) and mean MTR_{asym} (f). In d-f, the mean \pm SD from triplicate digestion experiments is shown.

volume. We note that for the present goal of jointly measuring MT and CEST effects under acquisition conditions suitable for *in vivo* scanning, we have used different values of B_1 amplitude, T_{sat} and Δ (see Section 2.5) as reported in our previous work (Mayar et al., 2022) for obtaining the MTR parameter. However, as the latter parameter is semi-quantitative and its value depends on the acquisition parameters (Henkelman et al., 2001), based on our previous work (Mayar et al., 2022) we estimate that a stronger distinction between USM and HSM

systems could be achieved by using higher B_1 , longer T_{sat} and larger Δ values.

The MTR maps of the bottom slice, shown in supplementary Fig. S2 which consists mainly of protein coagulum, show that for HSM the total amount of coagulum and the average MTR inside the coagulum increased between $t = 1$ and 15 min and decreased from $t = 15$ –60 min. This suggests that during the digestion process, the protein coagulum changed from a loose and porous structure at $t = 1$ min to a more

compact structure at $t = 15$ min, with consequent pepsin-induced breakdown. Moreover, a better distinction between USM and HSM can be made based on the MTR of the bottom slice. This is especially evident at $t = 15$ min, at which a two-fold higher MTR and a more compact coagulum was found for HSM compared to USM. Therefore, spatially-resolved measurements of the MTR can be used to monitor the coagulum volume as well as structural changes inside the coagulum during the digestion process. In our previous work we have shown that the MTR is governed by the amount of semi-solid material and by the accessibility of semi-solid protein protons to surrounding labile protons (Mayar et al., 2022). This also implies that the MTR does not provide any information on protein digestion in the absence of a semi-solid component, which is evident from the data for intestinal digestion (Fig. 5a and b, bottom).

To monitor digestion of soluble proteins/peptides, a different contrast is needed. The MTR_{asym} maps for USM during gastric digestion (Fig. 5c, top) mainly show an increase in the supernatant volume with digestion, but no increase in the MTR_{asym} of the supernatant is observed. However, for HSM during both gastric and intestinal digestion, a clear increase in the MTR_{asym} of the supernatant is observed in the contrast maps (Fig. 5c, middle and bottom) and in the evolution of the MTR_{asym} with the digestion time (Fig. 5f). This increase can be the result of protein solubilization and hydrolysis. The latter is expected to occur only for heated milk, in which the whey proteins are denatured and, therefore, more susceptible to protein hydrolysis by pepsin. This was previously reported by Sánchez-Rivera et al. (2015), who showed that the amount of intact β -lactoglobulins decreased more rapidly during dynamic *in vitro* digestion for HSM compared to USM (Sánchez-Rivera et al., 2015). A combination of semi-solid protein solubilization and whey protein hydrolysis is expected to result in more exchangeable protons, including amine protons, thereby explaining the higher variation of the MTR_{asym} at $\Delta = \pm 2.7$ ppm observed for HSM compared to USM during *in vitro* gastric digestion.

The MTR_{asym} values of intestinal digestion are lower than those of gastric digestion because for the intestinal phase, the last time point of the gastric phase ($t = 60$ min) was mixed with SIF, resulting in a dilution of the total amount of protein in the sample. The solubilized proteins and large peptides produced during gastric digestion are further hydrolyzed into smaller peptides during intestinal digestion (Zenker et al., 2020). The MTR_{asym} increased by 80% over the first 15 min of intestinal digestion, and thereafter reached a stable value up to 60 min.

The observed increase in the MTR_{asym} can be attributed to protein hydrolysis, because both $pH \sim 6.6 \pm 0.3$ and protein concentration remained constant during the static intestinal digestion experiment, during which no phase separation had occurred and the full digestion sample was measured.

Overall, these results demonstrate that T_2 -, MTR and MTR_{asym} contrast are complementary and can be used to probe different events that occur during protein digestion, respectively changes in the semi-solid and liquid volume, formation and degradation of the protein coagulum and its accessibility to water and molecular-level hydrolysis of soluble proteins. The latter makes the MTR_{asym} suitable for monitoring protein hydrolysis at later stages of digestion.

Measurements of water relaxation rates have also shown great potential for monitoring digestion of protein gels (Deng et al., 2020, 2022). However, the major limitation of 1H relaxometry is that it cannot measure low-abundant and semi-solid macromolecules, because it lacks dynamic range, short (sub-ms) relaxation times cannot be assessed with clinical scanners and/or their fitting error is too high. 1H MT and CEST, although affected by relaxation, enable circumventing these limitations, are inherently chemically-specific and are fast enough to be feasible *in vivo*. In addition, semi-quantitative parameters (MTR and MTR_{asym}) do not require any fitting procedures. While relaxometry can be made chemically specific, this would lengthen the measurement time, thereby hindering *in vivo* feasibility. In addition, it has been shown that the R_2 is not sensitive to the hydrolysis of whey proteins in solution (Deng et al.,

2020), while in this article we have shown that the MTR_{asym} is sensitive to protein breakdown in solution during the hydrolysis of a WPC solution (Fig. 2) and during intestinal digestion of skim milk (Fig. 5).

The work presented here, as well as our previous work (Mayar et al., 2022), were the first steps in exploring the potential of 1H CEST and MT measurements for monitoring *in vitro* and *in vivo* protein digestion. The next step is to apply these methods to monitor milk protein digestion under dynamic *in vitro* and *in vivo* digestion conditions, where in addition to protein solubilization and hydrolysis, large variations in pH and protein concentration (Mulet-Cabero, Egger, et al., 2020; Mulet-Cabero, Mackie, et al., 2020) are expected to occur due to gastric secretion and emptying. Moreover, the measurement temperature for dynamic *in vitro* and *in vivo* studies will be $37^\circ C$ compared to RT used in this work. A more complete validation of the method for monitoring dynamic gastric digestion would need to additionally account for pH, concentration and temperature effects on the chemical exchange.

For future dynamic *in vitro* and *in vivo* applications, the optimized 1H MT and CEST characterization methods must be validated on a clinical MRI scanner, where inhomogeneities in both static (B_0) and radio frequency (B_1) magnetic fields are expected to affect the saturation and, hence, the MT and CEST response. In this work, we used the WASSR approach to correct for B_0 inhomogeneities, which is too time consuming for dynamic applications. We foresee that fast B_0 - and B_1 -mapping procedures combined with regression- or two-pool Lorentzian modeling-based approaches for correction of sparsely sampled CEST data (Chen et al., 2022; Sun, 2020) will be a key requirement for robust analysis and interpretation of the CEST data. Another challenge of *in vivo* measurements is that breathing can cause breathing-related artifacts in the images, therefore, each scan should be conducted within one breath hold (≤ 20 s), which is possible with the acquisition parameters presented here. Moreover, we expect that image registration of all scans obtained at each digestion time point ($S_{sat}(\pm\Delta)$, S_0 , B_0 and B_1 map) will be crucial to avoid motion induced artifacts in the calculated MTR and MTR_{asym} maps.

4. Conclusions

In this work, we successfully applied 1H CEST MRI measurements to monitor the *in vitro* digestion of milk proteins. More specifically, we showed that the MTR_{asym} area can be used for probing the static *in vitro* gastric digestion of unheated and heated skim milk. There was an effect of digestion time ($p < 0.001$) and heat treatment ($p < 0.005$) on the MTR_{asym} area. The MTR_{asym} area increased during digestion, indicating an increase in free amine and hydroxyl groups due to protein solubilization and hydrolysis. In addition, we showed that a combination of T_2 -, MTR - and MTR_{asym} -contrast maps obtained within a short (1.3 min) measurement time can be used to monitor macroscopic changes in the protein coagulum and hydrolysis of soluble proteins during static *in vitro* gastro-intestinal digestion. Our findings open the way to future non-invasive monitoring of *in vitro* and *in vivo* protein digestion by means of MT- and CEST-based MRI techniques.

Funding

This work was supported by the Dutch Ministry of Economic Affairs Top Sector Agri&Food [grant number AF-18012, Effect of processing on digestion & immunogenicity of proteins in infant nutrition].

Declaration of Competing Interest

The authors declare the following financial interests/personal relationships which may be considered as potential competing interests: John van Duynhoven has an employment with a company (Unilever) that uses dairy ingredients to manufacture food products. The other authors declare that they have no known competing financial interests.

Acknowledgements

Luisa Ciobanu and Julien Flament are gratefully acknowledged for providing the CEST-RARE pulse sequence. Julie Miltenburg is gratefully acknowledged for providing the whey protein concentrate. Camilla Terenzi acknowledges funding from the 4TU Precision Medicine program supported by High Tech for a Sustainable Future. We also acknowledge the support of NWO for the MAGNEFY centre, which is part of the uNMR-NL national facility (NWO grant 184.032.207).

Appendix A. Supporting information

Supplementary data associated with this article can be found in the online version at doi:10.1016/j.foosr.2023.100314.

References

- Barbé, F., Le Feunteun, S., Rémond, D., Ménard, O., Jardin, J., Henry, G., Laroche, B., & Dupont, D. (2014). Tracking the in vivo release of bioactive peptides in the gut during digestion: Mass spectrometry peptidomic characterization of effluents collected in the gut of dairy matrix fed mini-pigs. *Food Research International*, 63 (September 2014), 147–156. <https://doi.org/10.1016/j.foodres.2014.02.015>
- Bhat, M. Y., Dar, T. A., & Singh, L. R. (2016). Casein proteins: Structural and functional aspects (Issue September). *Milk proteins - From structure to biological properties and health aspects* (1st ed, pp. 1–18). IntechOpen. <https://doi.org/10.5772/64187> (Issue September).
- Bos, C., Metges, C. C., Gaudichon, C., Petzke, K. J., Pueyo, M. E., Morens, C., Everwand, J., Benamouzig, R., & Tomé, D. (2003). Postprandial kinetics of dietary amino acids are the main determinant of their metabolism after soy or milk protein ingestion in humans. *Journal of Nutrition*, 133(5), 1308–1315. <https://doi.org/10.1093/jn/133.5.1308>
- Brodtkorb, A., Egger, L., Alminger, M., Alvito, P., Assunção, R., Ballance, S., Bohn, T., Bourliew-Lacanal, C., Boutrou, R., Carrière, F., Clemente, A., Corredig, M., Dupont, D., Dufour, C., Edwards, C., Golding, M., Karakaya, S., Kirkhus, B., le Feunteun, S., & Recio, I. (2019). INFOGEST static in vitro simulation of gastrointestinal food digestion. *Nature Protocols*, 14(4), 991–1014. <https://doi.org/10.1038/s41596-018-0119-1>
- Camps, G., Eijnatten, E.J.M. Van, Lieshout, G.A.A. Van, Lambers, T.T., & Smeets, P.A.M. (2021). Gastric emptying and intragastric behavior of breast milk and infant formula in lactating mothers gastric emptying and intragastric behavior of breast milk and infant formula in lactating. September. <https://doi.org/10.1093/jn/nxab295>
- Camps, G., Mars, M., de Graaf, C., & Smeets, P. A. M. (2017). A tale of gastric layering and sieving: Gastric emptying of a liquid meal with water blended in or consumed separately. *Physiology and Behavior*, 176(December 2016), 26–30. <https://doi.org/10.1016/j.physbeh.2017.03.029>
- Chan, K. W. Y., Yu, T., Qiao, Y., Liu, Q., Yang, M., Patel, H., Liu, G., Kinzler, K. W., Vogelstein, B., Bulte, J. W. M., Van Zijl, P. C. M., Hanes, J., Zhou, S., & McMahon, M. T. (2014). A diCEST MRI approach for monitoring liposomal accumulation in tumors. *Journal of Controlled Release*, 180(1), 51–59. <https://doi.org/10.1016/j.jconrel.2014.02.005>
- Chen, Y., Dang, X., Zhao, B., Zheng, Z., He, X., & Song, X. (2022). B0 correction for 3T Amide Proton Transfer (APT) MRI using a simplified two-pool lorentzian model of symmetric water and asymmetric solutes. *Tomography*, 8, 1974–1986.
- Cornacchia, L., Forquenot De La Fortelle, C., & Venema, P. (2014). Heat-induced aggregation of whey proteins in aqueous solutions below their isoelectric point. *Journal of Agricultural and Food Chemistry*, 62(3), 733–741. <https://doi.org/10.1021/jf404456q>
- DeBrosse, C., Nanga, R. P. R., Bagga, P., Nath, K., Haris, M., Marincola, F., Schnall, M. D., Hariharan, H., & Reddy, R. (2016). Lactate chemical exchange saturation transfer (LATEST) imaging in vivo a biomarker for LDH activity. *Scientific Reports*, 6 (January), 1–10. <https://doi.org/10.1038/srep19517>
- Deng, R., Janssen, A. E. M., Vergeldt, F. J., van As, H., de Graaf, C., Mars, M., & Smeets, P. A. M. (2020). Exploring in vitro gastric digestion of whey protein by time-domain nuclear magnetic resonance and magnetic resonance imaging. *Food Hydrocolloids*, 99(August 2019), Article 105348. <https://doi.org/10.1016/j.foodhyd.2019.105348>
- Deng, R., Seimys, A., Mars, M., Janssen, A. E. M., & Smeets, P. A. M. (2022). Monitoring pH and whey protein digestion by TD-NMR and MRI in a novel semi-dynamic in vitro gastric simulator (MR-GAS). *Food Hydrocolloids*, 125, Article 107393. <https://doi.org/10.1016/j.foodhyd.2021.107393>
- Dong, L., Wu, K., Cui, W., Fu, D., Han, J., & Liu, W. (2021). Tracking the digestive performance of different forms of dairy products using a dynamic artificial gastric digestive system. *Food Structure*, 29(May), Article 100194. <https://doi.org/10.1016/j.foosr.2021.100194>
- Dupont, D., & Tomé, D. (2014). Milk proteins: Digestion and absorption in the gastrointestinal tract. In M. Boland, & H. Singh (Eds.), *Milk proteins from expression to food* (3rd ed, pp. 701–714). Academic Press. <https://doi.org/10.1016/B978-0-12-405171-3.00020-9>
- Dupont, D., & Tomé, D. (2019). Milk proteins: Digestion and absorption in the gastrointestinal tract. *Milk proteins* (3rd ed, pp. 701–714). Academic Press. <https://doi.org/10.1016/B978-0-12-815251-5.00020-7>
- Gan, J., Bornhorst, G. M., Henrick, B. M., & German, J. B. (2018). Protein digestion of baby foods: Study approaches and implications for infant health. *Molecular Nutrition and Food Research*, 62(1), 1–11. <https://doi.org/10.1002/mnfr.201700231>
- Gaudichon, C., Mahé, S., Benamouzig, R., Luengo, C., Fouillet, H., Daré, S., Van Oycye, M., Ferrière, F., Rautureau, J., & Tomé, D. (1999). Net postprandial utilization of [15N]-labeled milk protein nitrogen is influenced by diet composition in humans. *Journal of Nutrition*, 129(4), 890–895. <https://doi.org/10.1093/jn/129.4.890>
- Goerke, S., Zaiss, M., Kunz, P., Klika, K. D., Windschuh, J. D., Mogk, A., Bukau, B., Ladd, M. E., & Bachert, P. (2015). Signature of protein unfolding in chemical exchange saturation transfer imaging. *NMR in Biomedicine*, 28(7), 906–913. <https://doi.org/10.1002/nbm.3317>
- Henkelman, R. M., Huang, X., Xiang, Q. -S., Stanisz, G. J., Swanson, S. D., & Bronskill, M. J. (1993). Quantitative interpretation of magnetization transfer. *Magnetic Resonance in Medicine*, 29(6), 759–766. <https://doi.org/10.1002/mrm.1910290607>
- Henkelman, R. M., Stanisz, G. J., & Graham, S. J. (2001). Magnetization transfer in MRI: A review. *NMR in Biomedicine*, 14(2), 57–64. <https://doi.org/10.1002/nbm.683>
- Horstman, A. M. H., Ganzevles, R. A., Kudla, U., Kardinaal, A. F. M., van den Borne, J. J. G. C., & Huppertz, T. (2021). Postprandial blood amino acid concentrations in older adults after consumption of dairy products: The role of the dairy matrix. *International Dairy Journal*, 113, Article 104890. <https://doi.org/10.1016/j.idairyj.2020.104890>
- Huppertz, T., & Chia, L. W. (2021). Milk protein coagulation under gastric conditions: A review. *International Dairy Journal*, 113, Article 104882. <https://doi.org/10.1016/j.idairyj.2020.104882>
- Kim, M., Gillen, J., Landman, B. A., Zhou, J., & Van Zijl, P. C. M. (2009). Water saturation shift referencing (WASSR) for chemical exchange saturation transfer (CEST) experiments. *Magnetic Resonance in Medicine*, 61(6), 1441–1450. <https://doi.org/10.1002/mrm.21873>
- Longo, D. L., Di Gregorio, E., Abategiovanni, R., Ceccon, A., Assfalg, M., Molinari, H., & Aime, S. (2014a). Chemical exchange saturation transfer (CEST): An efficient tool for detecting molecular information on proteins' behaviour. *Analyst*, 139(11), 2687–2690. <https://doi.org/10.1039/c4an00346b>
- Longo, D. L., Di Gregorio, E., Abategiovanni, R., Ceccon, A., Assfalg, M., Molinari, H., & Aime, S. (2014b). Chemical exchange saturation transfer (CEST): An efficient tool for detecting molecular information on proteins' behaviour. *Analyst*, 139(11), 2687–2690. <https://doi.org/10.1039/c4an00346b>
- Markoska, T., Daniloski, D., Vasiljevic, T., & Huppertz, T. (2021). Structural changes of β-casein induced by temperature and pH analysed by nuclear magnetic resonance, fourier-transform infrared spectroscopy, and chemometrics. *Molecules*, 26(24). <https://doi.org/10.3390/molecules26247650>
- Mayar, M., Miltenburg, J. L., Hettinga, K., Smeets, P. A. M., van Duynhoven, J. P. M., & Terenzi, C. (2022). Non-invasive monitoring of in vitro gastric milk protein digestion kinetics by 1H NMR magnetization transfer. *Food Chemistry*, 383(February), Article 132545. <https://doi.org/10.1016/j.foodchem.2022.132545>
- Ménard, O., Bourliew, C., de Oliveira, S. C., Dellarosa, N., Laghi, L., Carrière, F., Capozzi, F., Dupont, D., & Deglaire, A. (2018). A first step towards a consensus static in vitro model for simulating full-term infant digestion. *Food Chemistry*, 240(2017), 338–345. <https://doi.org/10.1016/j.foodchem.2017.07.145>
- Mulet-Cabero, A. I., Egger, L., Portmann, R., Ménard, O., Marze, S., Minekus, M., le Feunteun, S., Sarkar, A., Grundy, M. M. L., Carrière, F., Golding, M., Dupont, D., Recio, I., Brodtkorb, A., & Mackie, A. (2020). A standardised semi-dynamic: In vitro digestion method suitable for food-an international consensus. *Food and Function*, 11 (2), 1702–1720. <https://doi.org/10.1039/c9fo01293a>
- Mulet-Cabero, A. I., Mackie, A. R., Brodtkorb, A., & Wilde, P. J. (2020). Dairy structures and physiological responses: A matter of gastric digestion. *Critical Reviews in Food Science and Nutrition*, 60(22), 3737–3752. <https://doi.org/10.1080/10408398.2019.1707159>
- Mulet-Cabero, A. I., Rigby, N. M., Brodtkorb, A., & Mackie, A. R. (2017). Dairy food structures influence the rates of nutrient digestion through different in vitro gastric behaviour. *Food Hydrocolloids*, 67, 63–73. <https://doi.org/10.1016/j.foodhyd.2016.12.039>
- Nielsen, P. M., Petersen, D., & Dambmann, C. (2001). Improved method for determining food protein degree of hydrolysis. *Journal of Food Science*, 66(5), 642–646. <https://doi.org/10.1111/j.1365-2621.2001.tb04614.x>
- Nielsen, S. D., Beverly, R. L., Underwood, M. A., & Dallas, D. C. (2020). Differences and similarities in the peptide profile of preterm and term mother's milk, and preterm and term infant gastric samples. *Nutrients*, 12, 2825–2839.
- Pardi, A., Wagner, G., & Wutrich, K. (1983). Protein conformation and proton nuclear-magnetic-resonance chemical shifts. *European Journal of Biochemistry*, 137(3), 445–454. <https://doi.org/10.1111/j.1432-1033.1983.tb07848.x>
- Sánchez-Rivera, L., Ménard, O., Recio, I., & Dupont, D. (2015). Peptide mapping during dynamic gastric digestion of heated and unheated skimmed milk powder. *Food Research International*, 77, 132–139. <https://doi.org/10.1016/j.foodres.2015.08.001>
- Smeets, P. A. M., Deng, R., van Eijnatten, E. J. M., & Mayar, M. (2020). Monitoring food digestion with magnetic resonance techniques. *Proceedings of the Nutrition Society*, 3, 1–11. <https://doi.org/10.1017/S0029665120007867>
- Spellman, D., McEvoy, E., O'Cuinn, G., & FitzGerald, R. J. (2003). Proteinase and exopeptidase hydrolysis of whey protein: Comparison of the TNBS, OPA and pH stat methods for quantification of degree of hydrolysis. *International Dairy Journal*, 13(6), 447–453. [https://doi.org/10.1016/S0958-6946\(03\)00053-0](https://doi.org/10.1016/S0958-6946(03)00053-0)
- Spiller, R., & Marciari, L. (2019). Intraluminal impact of food: New insights from MRI. *Nutrients*, 11(5), 1147–1161. <https://doi.org/10.3390/nu11051147>
- Sun, P. Z. (2020). Fast correction of B0 field inhomogeneity for pH-specific magnetization transfer and relaxation normalized amide proton transfer imaging of

- acute ischemic stroke without Z-spectrum. *Magnetic Resonance in Medicine*, 83(5), 1688–1697. <https://doi.org/10.1002/mrm.28040>
- Sun, P. Z., Xiao, G., Zhou, I. Y., Guo, Y., & Wu, R. (2016). A method for accurate pH mapping with chemical exchange saturation transfer (CEST) MRI. *Contrast Media and Molecular Imaging*, 11(3), 195–202. <https://doi.org/10.1002/cmmi.1680>
- van Duynhoven, J. P. M., Kulik, A. S., Jonker, H. R. A., & Haverkamp, J. (1999). Solid-like components in carbohydrate gels probed by NMR spectroscopy. *Carbohydrate Polymers*, 40(3), 211–219. [https://doi.org/10.1016/S0144-8617\(99\)00056-9](https://doi.org/10.1016/S0144-8617(99)00056-9)
- van Lieshout, G. A. A., Lambers, T. T., Bragt, M. C. E., & Hettinga, K. A. (2020). How processing may affect milk protein digestion and overall physiological outcomes: A systematic review. *Critical Reviews in Food Science and Nutrition*, 60(14), 2422–2445. <https://doi.org/10.1080/10408398.2019.1646703>
- van Zijl, P. C. M., Lam, W. W., Xu, J., Knutsson, L., & Stanis, G. J. (2018). Magnetization Transfer Contrast and Chemical Exchange Saturation Transfer MRI. Features and analysis of the field-dependent saturation spectrum. *NeuroImage*, 168, 222–241. <https://doi.org/10.1016/j.neuroimage.2017.04.045>
- Van Zijl, P. C. M., & Yadav, N. N. (2011). Chemical exchange saturation transfer (CEST): What is in a name and what isn't? *Magnetic Resonance in Medicine*, 65(4), 927–948. <https://doi.org/10.1002/mrm.22761>
- Wu, B., Warnock, G., Zaiss, M., Lin, C., Chen, M., Zhou, Z., Mu, L., Nanz, D., Tuura, R., & Delso, G. (2016). An overview of CEST MRI for non-MR physicists. *EJNMMI Physics*, 3(1). <https://doi.org/10.1186/s40658-016-0155-2>
- Zenker, H. E., Van Lieshout, G. A. A., Van Gool, M. P., Bragt, M. C. E., & Hettinga, K. A. (2020). Lysine blockage of milk proteins in infant formula impairs overall protein digestibility and peptide release. *Food and Function*, 11(1), 358–369. <https://doi.org/10.1039/c9fo02097g>